

---

---

# Utility of $^{211}\text{At}$ -Trastuzumab for the Treatment of Metastatic Gastric Cancer in the Liver: Evaluation of a Preclinical $\alpha$ -Radioimmunotherapy Approach in a Clinically Relevant Mouse Model

Huizi Keiko Li<sup>1</sup>, Yukie Morokoshi<sup>1</sup>, Satoshi Kodaira<sup>2</sup>, Tamon Kusumoto<sup>2</sup>, Katsuyuki Minegishi<sup>3</sup>, Hiroaki Kanda<sup>4</sup>, Kotaro Nagatsu<sup>3</sup>, and Sumitaka Hasegawa<sup>1</sup>

<sup>1</sup>Radiation and Cancer Biology Group, National Institutes for Quantum and Radiological Science and Technology, Chiba, Japan;

<sup>2</sup>Radiation Measurement Research Group, National Institutes for Quantum and Radiological Science and Technology, Chiba, Japan;

<sup>3</sup>Targetry and Target Chemistry Group, National Institutes for Quantum and Radiological Science and Technology, Chiba, Japan; and

<sup>4</sup>Department of Pathology, Saitama Cancer Center, Saitama, Japan

---

J Nucl Med 2021; 62:1468–1474

DOI: 10.2967/jnumed.120.249300

---

A liver metastasis from a primary gastric cancer (LMGC) is relatively common and results in an extremely poor prognosis due to a lack of effective therapeutics. We here demonstrate in a clinically relevant mouse model that an  $\alpha$ -particle radioimmunotherapy approach with  $^{211}\text{At}$ -labeled trastuzumab has efficacy against LMGCs that are positive for human epidermal growth factor receptor 2 (HER2). **Methods:**  $^{211}\text{At}$  was produced in a cyclotron via a  $^{209}\text{Bi}(\alpha, 2n)^{211}\text{At}$  reaction.  $^{211}\text{At}$ -trastuzumab was subsequently generated using a single-step labeling method. NCI-N87 cells (HER2-positive human gastric cancer cells) carrying a luciferase gene were intrasplenically transplanted into severe combined immunodeficiency mice to generate an HER2-positive LMGC model. A biodistribution study was then conducted through the intravenous injection of  $^{211}\text{At}$ -trastuzumab (1 MBq) into these LMGC xenograft mice. In parallel with this experimental therapy, phosphate-buffered saline, intact trastuzumab, or  $^{211}\text{At}$ -nonspecific human IgG (1 MBq) was injected into control groups. The therapeutic efficacy was evaluated by monitoring tumor changes by chemiluminescence imaging. Body weights, white blood cell counts, and serum markers of tissue damage were monitored at regular intervals. Microdosimetry using a CR-39 plastic detector was also performed. **Results:** The biodistribution analysis revealed an increased uptake of  $^{211}\text{At}$ -trastuzumab in the metastasized tumors that reached approximately 12% of the injected dose per gram of tissue (%ID/g) at 24 h. In contrast, its uptake to the surrounding liver was about 4 %ID/g. The LMGCs in the mouse model reduced dramatically at 1 wk after the single systemic injection of  $^{211}\text{At}$ -trastuzumab. No recurrences were observed in 6 of 8 mice treated with this single injection, and their survival time was significantly prolonged compared with the control groups, including the animals treated with  $^{211}\text{At}$ -nonspecific antibodies. No severe toxicities or abnormalities in terms of body weight, white blood cell number, liver function, or kidney parameters were observed in the  $^{211}\text{At}$ -trastuzumab group. Microdosimetric studies further revealed that  $^{211}\text{At}$ -trastuzumab had been delivered at an 11.5-fold higher dose to the LMGC lesions than to the normal liver. **Conclusion:**  $\alpha$ -radioimmunotherapy with  $^{211}\text{At}$ -trastuzumab has considerable potential as an effective and safe therapeutic option for LMGC.

**Key Words:** cancer metastasis; gastric cancer; HER2;  $\alpha$ -RIT

---

Received May 8, 2020; revision accepted Jan. 13, 2021.

For correspondence or reprints, contact Sumitaka Hasegawa (hasegawa.sumitaka@qst.go.jp).

Published online February 5, 2021.

COPYRIGHT © 2021 by the Society of Nuclear Medicine and Molecular Imaging.

**G**astric cancer (GC) is the fifth most frequently diagnosed cancer and the third leading cause of cancer-related death worldwide (1). Significantly, 35% of GC patients develop a distant metastasis at the time of diagnosis, with 4%–14% of GCs developing a liver metastasis (liver metastasis from a primary GC, or LMGC) (2). No satisfactory therapeutics have yet been established for LMGCs, and the prognosis is therefore dismal, with a 5-y survival rate of 0%–10%. Human epidermal growth factor receptor 2 (HER2) has shown promise as a therapeutic target for GC, as HER overexpression is observed in 7%–34% of patients (3). Of note in this regard, previous studies have reported a higher HER2 positivity in LMGCs (37.2%) and a correlation of this overexpression with the poor prognosis in these patients (4,5). Indeed, a recombinant humanized monoclonal antibody targeting the HER2 protein, trastuzumab, has now been clinically used for HER2-overexpressing GCs (6). However, despite the clinical benefits of this drug in combination with chemotherapy, the long-term survival of LMGC patients remains unsatisfactory (7).

$\alpha$ -particle radioimmunotherapy ( $\alpha$ -RIT) is a targeted radionuclide treatment regimen that uses monoclonal antibodies for the specific delivery of radionuclide-emitting  $\alpha$ -particles (8).  $^{211}\text{At}$  is one of the currently attractive  $\alpha$ -particle emitters in terms of clinical use because it has an appropriate half-life (7.2 h) and can be manufactured using a cyclotron (9). Our prior preclinical studies in mouse models have provided evidence that  $^{211}\text{At}$ -labeled antibodies are effective against several cancers without severe toxic effects (10,11). The therapeutic effectiveness of  $^{211}\text{At}$ -labeled trastuzumab has been reported (12,13). Furthermore, the benefit of single-domain antibody fragments targeting HER2 has been studied (14).

We hypothesized that a targeted delivery of  $\alpha$ -particles using a cancer-specific antibody would have therapeutic efficacy against LMGC. We thus investigated the use of  $^{211}\text{At}$ -trastuzumab against HER2-overexpressing LMGCs in a preclinical mouse model.

## MATERIALS AND METHODS

### Cells and Reagents

The human NCI-N87 (N87) cell line was purchased from ATCC and was transfected with RediFect Red-FLuc-Puromycin lentiviral particles to establish N87 cells carrying luciferase genes (N87/Luc), as described previously (13). The MKN45-Luc (MKN45/Luc) cells were obtained from the Japanese Collection of Research Bioresources Cell Bank. Cells were cultured in RPMI-1640 medium, supplemented with 10% fetal bovine serum and 1% penicillin-streptomycin (Wako), and maintained in a humidified atmosphere of 5% CO<sub>2</sub> at 37°C. The anti-HER2 monoclonal antibody trastuzumab and human IgG (HuIgG) were purchased from Chugai Pharmaceutical and Invitrogen, respectively. *N*-succinimidyl-3-(trimethylstannyl)benzoate was obtained from Santa Cruz Biotechnology and stored at -30°C. *N*-chlorosuccinimide was purchased from Tokyo Chemical Industry.

### Antibodies and Radiochemistry

<sup>211</sup>At was produced in a cyclotron via a <sup>209</sup>Bi ( $\alpha, 2n$ )<sup>211</sup>At reaction at the National Institute of Radiologic Sciences of the National Institutes for Quantum and Radiologic Science and Technology, as described previously (15). The <sup>211</sup>At labeling of antibodies was also performed in accordance with a previously described method (10). Briefly, antibodies (3–5 mg/mL in 0.2 M sodium carbonate buffer, pH 8.5) were conjugated with *N*-succinimidyl-3-(trimethylstannyl)benzoate, and this immunoconjugated preparation was isolated in phosphate-buffered saline using a Sephadex 50 spin column (GE Healthcare). The tin concentration of the immunoconjugates was determined by inductively coupled plasma mass spectrometry using an Agilent 7500a device (Yokogawa Analytic Systems) (16). Briefly, the protein solutions (100  $\mu$ L, 232.8–296.5  $\mu$ g of protein) were digested with 0.5 mL of nitric acid (Tama Chemicals) at 90°C for 30 min using a microwave oven, diluted with ultrapure water. Under our experimental conditions, the quantitation limit of tin was 0.042 ng/g. The tin levels of trastuzumab or HuIgG without *N*-succinimidyl-3-(trimethylstannyl)benzoate in the solvent were below this quantitation limit. The immunoconjugate was then adjusted to pH 5.5 by adding citric acid before labeling. <sup>211</sup>At (55–90 MBq) was dissolved with a 0.04 mg/mL solution of *N*-chlorosuccinimide in methanol supplemented with 1% acetic acid for labeling. The immunoconjugate (2–3 mg/mL) was added to <sup>211</sup>At and reacted for 1 min, followed by another 1-min reaction with a 2 mg/mL solution of *N*-chlorosuccinimide. Finally, sodium ascorbate (50 mg/mL) was added to stop the reaction. <sup>211</sup>At-labeled antibodies (<sup>211</sup>At-trastuzumab and <sup>211</sup>At-HuIgG) were isolated in phosphate-buffered saline using a Sephadex 50 spin column and verified by high-performance liquid chromatography.

### Animal Experiments

All animal experiments were approved by the Animal Care and Use Committee of the National Institute of Radiological Sciences at the National Institutes for Quantum and Radiological Science and Technology and complied with the institutional guidelines on animal care and handling.

### LMGC Xenograft Mouse Model

N87/Luc or MKN45/Luc cells ( $2 \times 10^6$  cells in 50  $\mu$ L of medium) were intrasplenically transplanted into C.B17/Icr-scid/scidJcl mice (CLEA Japan, Inc.) under anesthesia to form liver metastases via the splenic vein. The spleen was resected after transplantation to avoid tumor formation in the spleen.

### Biodistribution and Dose Estimation

Biodistribution studies were performed as described previously (10). Briefly, <sup>211</sup>At-trastuzumab or <sup>211</sup>At-HuIgG (1 MBq/100  $\mu$ L) was intravenously injected into the LMGC xenograft mice. At 1, 3, and 24

h after injection, a group of 4–5 mice was euthanized and tumor and tissues were dissected. The activities in each tissue were measured using a  $\gamma$ -counter (Aloka) to calculate the percentage injected dose (%ID)/g. The absorbed dose of tumor and tissues were estimated as described previously (17). Briefly, the doses were estimated using the area under the curve on the basis of the biodistribution data (the trapezoidal method) and the mean energy emitted per transition of <sup>211</sup>At and a daughter nuclide <sup>211</sup>Po with a correction for the branching ratio (18). A radiation weighting factor of 5 was used (19).

### Experimental Therapy

The experimental therapy was performed by giving an injection of <sup>211</sup>At-trastuzumab (1 MBq) intravenously to the LMGC xenograft mice. Phosphate-buffered saline, intact trastuzumab, or <sup>211</sup>At-HuIgG (1 MBq) was also injected into control groups. All protein doses were adjusted to the equivalent amount (10  $\mu$ g) by adding intact antibody. The therapeutic efficacy was evaluated by monitoring tumor changes via chemiluminescence imaging. Body weights, white blood cell counts, and serum markers of tissue damage were monitored at regular intervals to evaluate the toxicity of the treatment. Mice were euthanized when the chemiluminescence intensity of the tumor reached  $1 \times 10^6$  or at 120 d after injection.

### Immunohistochemistry and Histologic Analysis

The HER2 expression level in the LMGCs was confirmed by immunohistochemical staining using a Histofine HER2 kit (Nichirei Biosciences) in accordance with the manufacturer's instructions. Histologic analysis was performed as described previously (10). Briefly, LMGC xenograft tissues were sampled from the mice at 1, 3, and 24 h after injection of <sup>211</sup>At-trastuzumab, fixed with 10% (v/v) formalin, and embedded in paraffin for sectioning. After sectioning, sequential samples were used for HER2 and hematoxylin and eosin staining.

### Microdosimetry

$\alpha$ -particle detection and microdosimetry were performed as described previously (20,21). Briefly, LMGC xenograft tissues containing a normal liver region were dissected at 24 h after the intravenous injection of <sup>211</sup>At-trastuzumab (1 MBq), filled with optimal-cutting-temperature compound, and sectioned at an 8- $\mu$ m thickness using a cryotome (Leica Biosystems). Sectioned samples were then placed on a CR-39 plate and exposed for 8 h at room temperature. During the exposure, the same sections were stained with hematoxylin and eosin, and histologic images were acquired using a scanning microscope with a  $\times 20$  objective lens. At 8 h after placement on CR-39, the samples were removed and the CR-39 plate was chemically etched for 2 h in 7 M sodium hydroxide solution at 70°C. Microscope images of the  $\alpha$ -particle tracks were captured under an FSP-1000 microscope (Seiko Time Systems Inc.) and analyzed with track analysis software (PitFit) (22).

### Statistical Analysis

Statcel 3 software (OMS) was used for all statistical analysis. Tumor volumes and survival data were analyzed using 2-way repeated measures ANOVA and the Kaplan–Meier method, respectively. A *P* value of less than 0.05 was considered significant.

## RESULTS

### Radiochemistry

The number of tin groups per antibodies measured using inductively coupled plasma mass spectrometry were  $5.2 \pm 0.1$  ( $n = 3$ ) and  $2.6 \pm 0.5$  ( $n = 3$ ) for trastuzumab and HuIgG immunoconjugates, respectively. The labeling yield and specific activity of our test molecules were  $51.6\% \pm 9.1\%$  and  $95.2\text{--}453.0$  kBq/ $\mu$ g for <sup>211</sup>At-trastuzumab and  $56.2\% \pm 9.7\%$  and  $19.9\text{--}521.7$  kBq/ $\mu$ g for

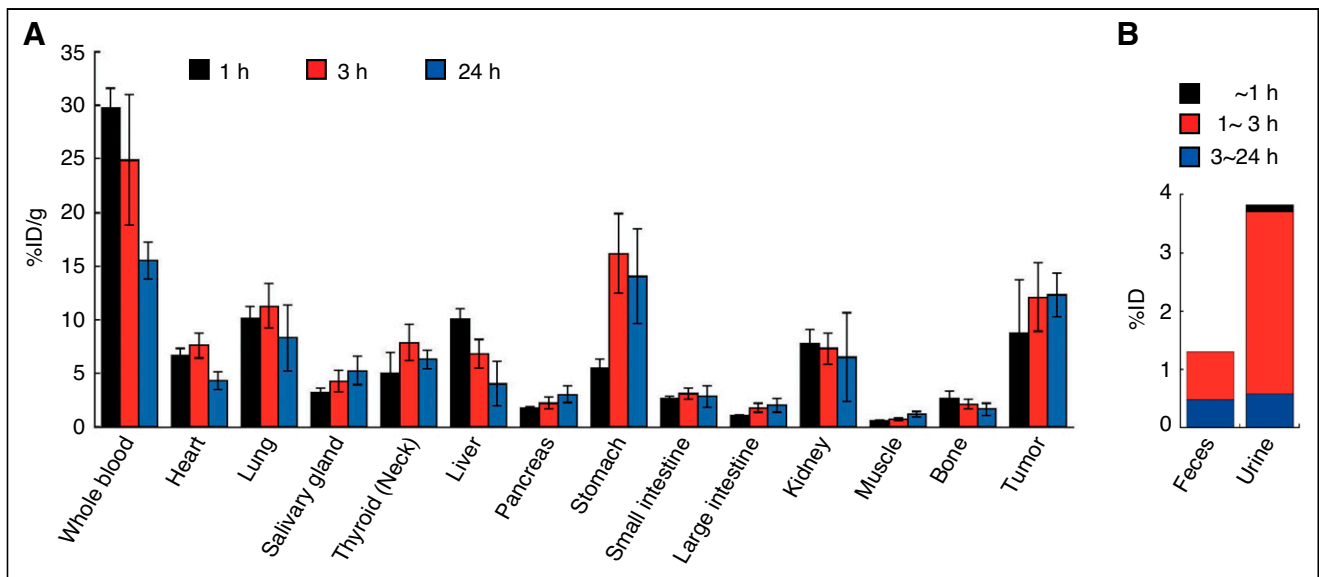


**FIGURE 1.** Biodistribution of  $^{211}\text{At}$ -trastuzumab in LMGC mouse model. (A) %ID/g for  $^{211}\text{At}$  in blood, organs, and tumor tissues at 1, 3, and 24 h after intravenous injection of  $^{211}\text{At}$ -trastuzumab (1 MBq). Data represent mean  $\pm$  SD ( $n = 5$  for each time point). (B) %ID of  $^{211}\text{At}$  in feces and urine of mice. Five animals were used at each time point. Data represent mean ( $n = 5$ ).

$^{211}\text{At}$ -HuIgG, respectively. The radiochemical purities of these agents were consistently measured above 95%.

#### Establishment of LMGC Mouse Model

An LMGC mouse model was established by transplanting N87/Luc or MKN45/Luc cells via the splenic vein into C.B17/Icr-scld/scldJcl mice (Supplemental Figs. 1 and 2; supplemental materials are available at <http://jnm.snmjournals.org>). LMGC lesions in this mouse model were confirmed both by chemiluminescence and visually (Supplemental Figs. 1A–1D). Immunohistochemical analyses confirmed the overexpression of HER2 in the LMGC lesions containing N87/Luc cells (Supplemental Figs. 1E and 1F).

#### Biodistribution and Absorbed Dose of $^{211}\text{At}$ -Trastuzumab in LMGC Mouse Model

Because the *in vitro* cell binding of  $^{211}\text{At}$ -trastuzumab to N87 cells and resulting cytotoxicity were reported previously (13), we investigated the biodistribution of this agent in our LMGC mice after the splenic vein implantation of N87/Luc cells into these animals. We measured longitudinal changes in the  $^{211}\text{At}$  uptake in each tissue and tumor after the mice received an intravenous injection of  $^{211}\text{At}$ -trastuzumab (1 MBq) (Fig. 1A). The tumor uptake was  $8.8 \pm 5.0$  %ID/g at 1 h after injection and increased over time up to  $12.3 \pm 2.0$  %ID/g at 24 h after injection. Because of its systemic administration,  $^{211}\text{At}$  uptake in the blood ( $29.8 \pm 1.8$  %ID/g), heart ( $6.7 \pm 0.7$  %ID/g), lung ( $10.2 \pm 1.1$  %ID/g), and liver ( $10.1 \pm 0.9$  %ID/g) was relatively higher than in other tissues at 1 h but then gradually decreased ( $15.6 \pm 1.7$ ,  $4.3 \pm 0.9$ ,  $8.3 \pm 3.1$ , and  $4.0 \pm 2.1$  %ID/g, respectively). Higher uptake in the thyroid and stomach ( $6.3 \pm 0.9$  and  $14.1 \pm 4.4$  %ID/g, respectively, at 24 h) was observed, likely because of free  $^{211}\text{At}$ . We further observed that  $^{211}\text{At}$ -trastuzumab was excreted mainly in the urine (3.8 %ID up to 24 h, Fig. 1B). The absorbed dose by each tissue was calculated from the biodistribution data (Table 1). The absorbed dose at the tumor was estimated to be 4.58 Gy up to 24 h after injection. The tumor-to-normal-liver ratio was 1.59, calculated from the biodistribution data. The  $^{211}\text{At}$  uptake decreased in the tumor at 24

h after the injection of  $^{211}\text{At}$ -trastuzumab, compared with a reduction after only 1 or 3 h in another LMGC model generated using MKN45/Luc cells that have a significantly lower HER2 expression level than N87/Luc cells (Supplemental Fig. 2). In addition,  $^{211}\text{At}$  uptake was found in our analysis to be decreased in the tumor at 24 h after the injection of  $^{211}\text{At}$ -HuIgG, compared with at only 1 or 3 h in the N87/Luc LMGC model (Supplemental Fig. 3).

#### Therapeutic Efficacy of $^{211}\text{At}$ -trastuzumab Against LMGC in Mouse Model

We next evaluated the therapeutic efficacy of  $\alpha$ -RIT using  $^{211}\text{At}$ -trastuzumab to treat LMGCs in our mouse model (Figs. 2 and

**TABLE 1**  
Absorbed Doses at 24 Hours after Intravenous Injection of  $^{211}\text{At}$ -Trastuzumab (1 MBq)

Tissue	Absorbed dose (Gy)
Whole blood	10.11
Heart	2.96
Lung	4.39
Salivary glands	1.61
Thyroid (neck)	2.95
Liver	2.88
Pancreas	0.85
Stomach	5.79
Small intestine	1.20
Large intestine	0.66
Kidney	2.90
Muscle	0.27
Bone	0.87
Tumor	4.58

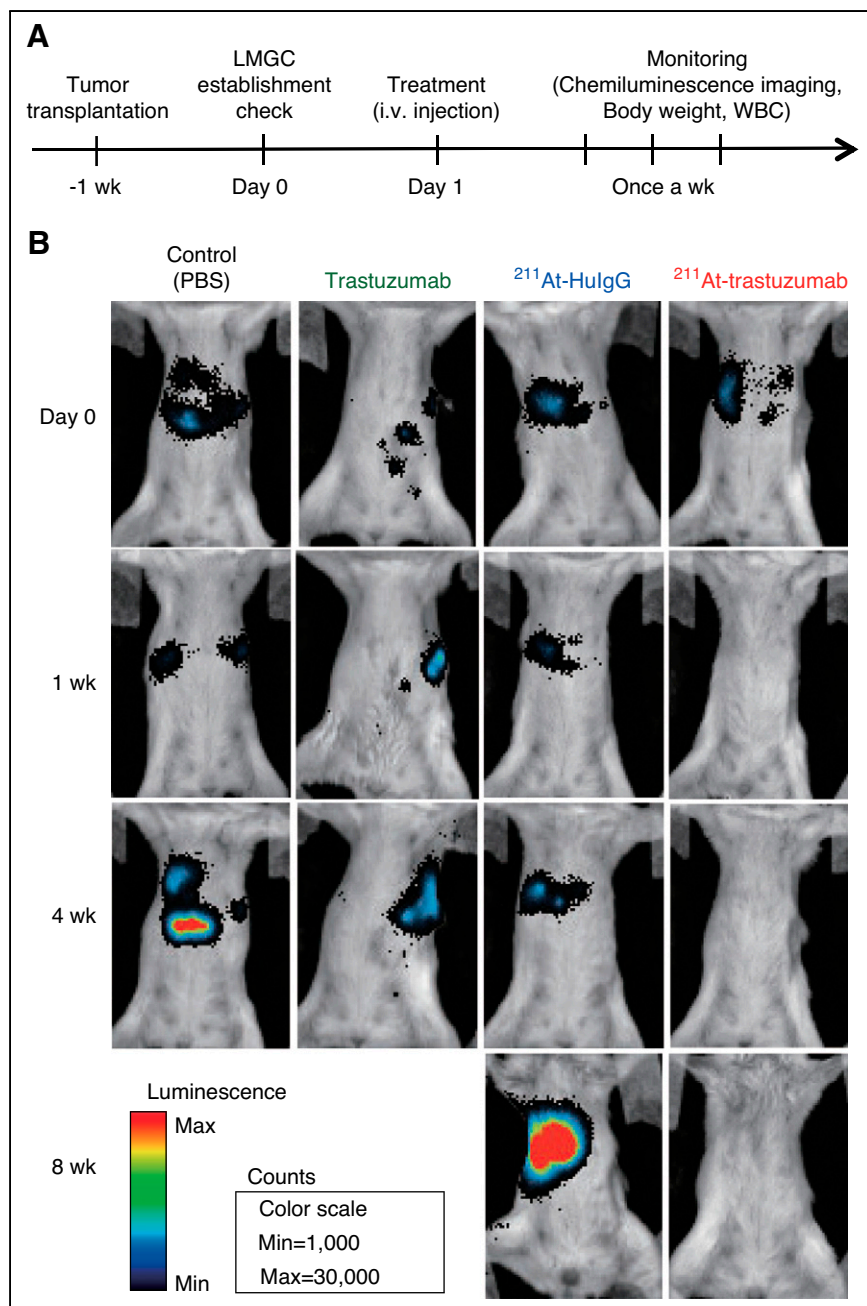


**FIGURE 2.**  $\alpha$ -RIT with  $^{211}\text{At}$ -trastuzumab in LMGC mouse model. (A) Treatment schema. (B) Representative chemiluminescence images of LMGC lesions in model mice on day before (day 0) and 1, 4, and 8 wk after treatment. Mice were treated with phosphate-buffered saline (PBS), trastuzumab (10  $\mu\text{g}$ ),  $^{211}\text{At}$ -HuIgG (1 MBq, 10  $\mu\text{g}$ ), or  $^{211}\text{At}$ -trastuzumab (1 MBq, 10  $\mu\text{g}$ ). Color scale indicates chemiluminescence intensity per pixel. i.v. = intravenous; WBC = white blood cell.

3). Chemiluminescence imagery revealed that a single injection of  $^{211}\text{At}$ -trastuzumab eradicated the LMGC lesions in the mice that received it, whereas these tumors grew aggressively in the animals that received control injections of phosphate-buffered saline, unlabeled trastuzumab, or  $^{211}\text{At}$ -HuIgG (Fig. 2B). The tumor changes at 28 d after treatment (Fig. 3A) and the relative chemiluminescence intensity of the LMGCs (Fig. 3B) indicated that these lesions were well controlled by the systemic injection of  $^{211}\text{At}$ -trastuzumab. No recurrences were observed in 6 of 8 mice treated

with a single injection of  $^{211}\text{At}$ -trastuzumab during the period of observation.  $^{211}\text{At}$ -trastuzumab also significantly prolonged the survival of the LMGC mice (Fig. 3C) compared with the control treatment groups. Histopathologic studies revealed necrotic lesions in both untreated and  $^{211}\text{At}$ -trastuzumab-treated LMGCs (Fig. 3D). However, the percentage of necrotic lesions in the tumors was higher in the  $^{211}\text{At}$ -trastuzumab-treated group.

#### Toxicity

We evaluated the toxicity levels of  $^{211}\text{At}$ -trastuzumab in the mouse model by monitoring body weight and conducting biochemical examinations of liver and kidney function. Body weight decreased immediately and started to recover about 1 wk after injection of either  $^{211}\text{At}$ -HuIgG or  $^{211}\text{At}$ -trastuzumab (Fig. 4A). No obvious leukocytopenia was observed during the period of observation (Fig. 4B). Biochemical examinations indicated no significant changes in the glutamic oxaloacetic transaminase, glutamic pyruvate transaminase, blood urea nitrogen, or creatinine levels before and after treatment (Fig. 4C). No atrophy, apoptosis, or noticeable damage was observed histopathologically in either the liver or the stomach at 3 h after  $\alpha$ -RIT treatment (Fig. 4D).

#### Microdosimetry

Figure 5 shows an intensity map of the  $\alpha$ -particle tracks emitted from  $^{211}\text{At}$  on the metastatic tumors in an LMGC mouse liver at 24 h after injection of  $^{211}\text{At}$ -trastuzumab. We extracted the tumor region of interest (Fig. 5A, dark pink) from a frozen section that included metastatic tumors by binarization by setting band-pass thresholds for the 24-bit color levels (red, 255; green, 163; blue, 173), and the number of  $\alpha$ -tracks located in the tumor region of interest in the tissue sample was counted in a binarized image (Fig. 5A). High-density  $\alpha$ -tracks were compared between the tumor region and the normal-tissue region; the numbers of  $\alpha$ -tracks per unit area of tumor and normal liver were  $49,849 \pm 975/\text{cm}^2$  and  $5,125 \pm 126/\text{cm}^2$ , respectively. The mean absorbed doses per section in the tumor and normal-tissue regions at 24 h were  $54.1 \pm 1.1$  and  $4.7 \pm 0.1$  mGy, respectively, suggesting that the tumor region received an 11.5-fold higher dose than the normal liver (Fig. 5B). This dosimetry was performed on an 8- $\mu\text{m}$ -thick tissue sample from which we visualized a very localized dose distribution in the section that distinguished the area in which the  $\alpha$ -particles were concentrated in the tumor.

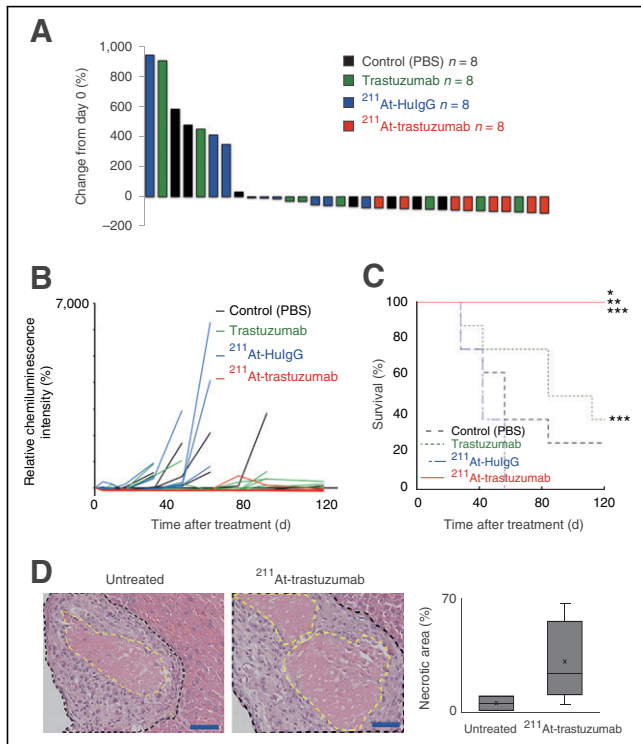


**FIGURE 3.** Results of  $^{211}\text{At-trastuzumab}$   $\alpha$ -RIT in LMGC mouse model. (A) Waterfall plot of percentage tumor chemiluminescence intensity change in each mouse at 28 d after treatment. Tumor chemiluminescence intensity at day 0 was set as baseline ( $n = 8$  in each group). (B) Relative chemiluminescence intensity of tumor in each mouse. Chemiluminescence intensity at day 0 was considered to be 100% ( $n = 8$  in each group). (C) Kaplan–Meier survival curves for LMGC mice. \* $P < 0.05$  vs. control. \*\* $P < 0.05$  vs. trastuzumab. \*\*\* $P < 0.05$  vs.  $^{211}\text{At-HulG}$  ( $n = 8$  in each group). (D) Histopathologic analysis by hematoxylin and eosin staining of LMGC lesions that were untreated and were treated for 3 h with  $\alpha$ -RIT. Scale bars = 50  $\mu\text{m}$ . Percentages of necrosis in tumors are shown at right. Two (for untreated) or 5 (for treated with  $^{211}\text{At-trastuzumab}$ ) mice were used. Data represent mean  $\pm$  SD. PBS = phosphate-buffered saline.

## DISCUSSION

The results of our present analysis indicate that a systemic injection of  $^{211}\text{At-trastuzumab}$  achieves dramatic tumor control in a clinically relevant mouse model of HER2-overexpressing LMGCs. In the mice treated with  $^{211}\text{At-trastuzumab}$ , the LMGCs were eradicated without recurrence during the monitored period in 6 of 8 animals. Previous studies have indicated that  $\alpha$ -particles induce huge clusters of irreparable DNA double-strand breaks and thereby cause targeted cancer cell death (10,11). Consistent with these findings, we found in our present analyses that broad necrotic lesions arise in LMGCs treated with  $^{211}\text{At-trastuzumab}$ . The survival of LMGC mice treated with  $^{211}\text{At-trastuzumab}$  was also significantly prolonged compared with the control-treated animals. These findings are particularly relevant because despite the continuing improvements in chemotherapy regimens, current treatments for LMGC patients are still limited in terms of extending survival, and the prognosis in these cases thus remains dismal. Hepatic resection and radiofrequency ablation are recommended in these cases if the metastasis is limited to the liver, but patients with LMGC often have multiple metastatic tumors in the liver and further metastases in the peritoneum, lymph nodes, and adjacent

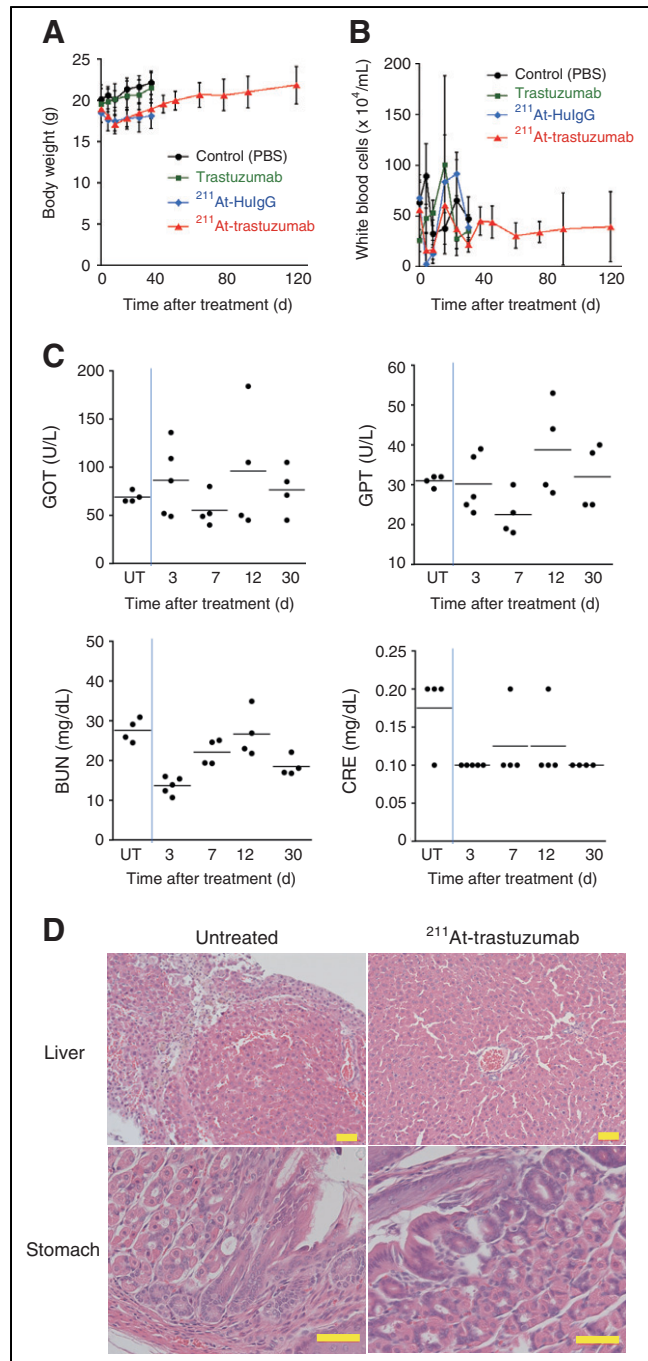


**FIGURE 4.** Toxicity evaluation of  $^{211}\text{At-trastuzumab}$   $\alpha$ -RIT in LMGC mouse model. (A and B) Body weights (A) and white blood cell counts (B) of LMGC mice after treatment are shown. Plots are interrupted if mouse reached endpoint. Data represent mean  $\pm$  SD. (C) Glutamic oxaloacetic transaminase (GOT), glutamic pyruvate transaminase (GPT), blood urea nitrogen (BUN), and creatinine (CRE) levels measured up to 30 d after  $^{211}\text{At-trastuzumab}$   $\alpha$ -RIT. Data for each mouse are shown in graph. (D) Histopathologic analysis by hematoxylin and eosin staining of mouse liver and stomach in animals that were untreated or treated with  $^{211}\text{At-trastuzumab}$  for 3 h with  $\alpha$ -RIT, respectively. Scale bars = 50  $\mu\text{m}$ . PBS = phosphate-buffered saline; UT = untreated mice.

organs (23–25). Hence, our current therapeutic strategy holds promise for the future management of LMGCs that are positive for HER2.

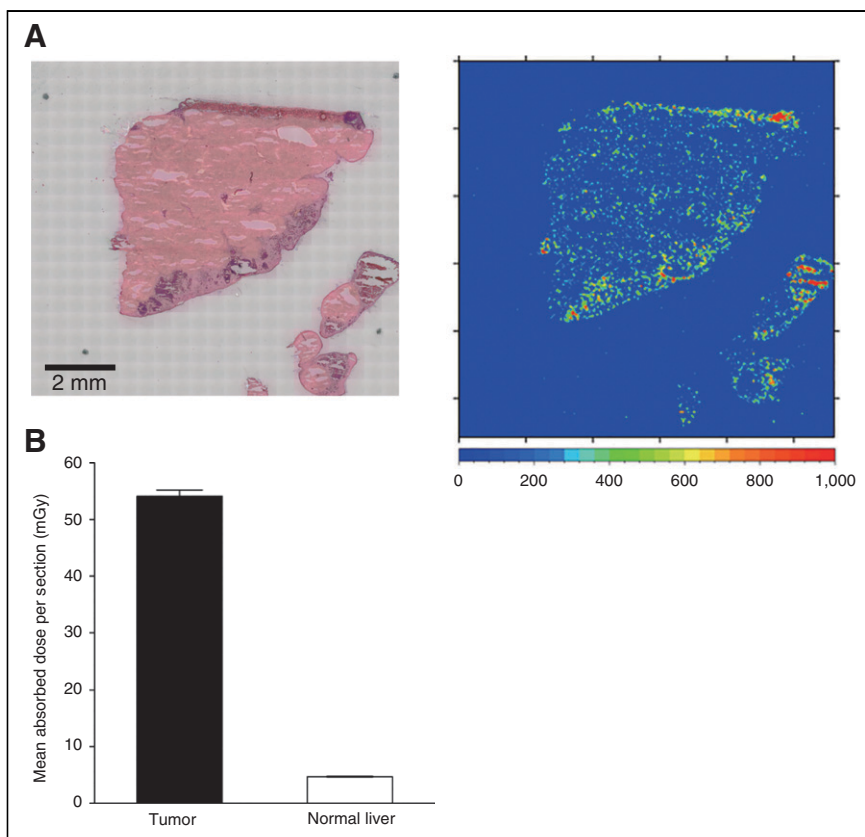


**FIGURE 5.** Microdosimetry. (A) Microscopic images of sectioned sample of mouse liver tissue, including metastasized tumors, and contour map of  $\alpha$ -particle track density at binned positions ( $\Delta X$ ,  $\Delta Y$ ) with 50- $\mu\text{m}$  intervals at 24 h after treatment. Scale bars = 2 mm. (B) Estimated local absorbed dose per frozen section at tumor and normal liver regions at 24 h after treatment.

Targeting  $\alpha$ -particle therapy or  $\alpha$ -RIT using  $^{211}\text{At}$  has been shown to be therapeutically effective for HER2-positive cancers in various mouse xenograft systems. For example,  $^{211}\text{At}$ -trastuzumab has been shown to be therapeutically effective in a mouse model of radioresistant ovarian cancer (12). A previous study reported the effectiveness of single-domain antibody fragments as an attractive platform for  $^{211}\text{At}$  delivery targeting HER2 because of their prolonged tumor targeting and rapid clearance from normal tissues (14). In addition,  $\alpha$ -emitters other than  $^{211}\text{At}$  are also used for  $\alpha$ -RIT against cancer.  $^{227}\text{Th}$ -labeled trastuzumab has shown significant therapeutic effects in a HER2-positive ovarian cancer xenograft (26). Recently also,  $\alpha$ -RIT using  $^{213}\text{Bi}$  has been shown to be effective for experimental pancreatic ductal adenocarcinoma (27).

Since  $\alpha$ -particles are highly cytotoxic, the safety of the  $\alpha$ -RIT approach is an important consideration for possible clinical applications. Damage to normal liver tissues will be one of the top issues of concern if this treatment approach is being tested for metastatic tumors in the liver. Hence, an effective and accurate dose estimation in the normal liver and metastatic tumors is of particular importance. We have here estimated the appropriate radiation dose for the normal liver and metastatic tumors using 2 different approaches: a biodistribution-based dose estimation and microdosimetry using a CR-39 plastic detector that we have previously reported (21). The tumor-to-liver ratios in the absorbed dose at 24 h after injection were 1.6 and 11.5 in the biodistribution-

based dose estimation and the microdosimetry, respectively (Table 1; Fig. 5B). LMGCs were carefully dissected to separate them from normal liver in the former approach, but normal liver tissues were inevitably mixed in with the LMGC samples measured, which would affect the result. Notably,  $^{211}\text{At}$  or  $^{211}\text{At}$ -trastuzumab would be expected to be localized in tissues with a nonhomogeneous distribution. Our microdosimetric analyses revealed that a 10-fold higher dose had been given to the tumor than to the normal liver, suggesting that the  $\alpha$ -particles had been successfully targeted using the antibody and that our strategy minimized the damage to the surrounding normal tissue (Fig. 5). This finding is highly relevant to the established and continuing concerns about systemic drug administration, including hematologic toxicity levels, damage to excretion pathways (liver and kidney), and the accumulation of free  $^{211}\text{At}$  in normal tissues.

Although a transient but recoverable loss of body weight was observed in our  $\alpha$ -RIT-treated LMGC mice, no apparent toxicities were evident over the monitoring period. Moreover, higher uptakes of  $^{211}\text{At}$ -trastuzumab were observed in the stomach (Fig. 1A), but we found no apparent histopathologic abnormalities (Fig. 4D). These

data support the safety of  $^{211}\text{At}$ -trastuzumab for translation to clinical use.

There were some limitations to this study. Although our LMGC model is highly relevant to the clinical manifestations of LMGC, the severe combined deficiency mice we used have, of course, severely defective immunity, and the effects of the immune system in tumor eradication via  $^{211}\text{At}$ -trastuzumab are unknown. Tumor-bearing mouse models with a functional immune system may be desirable for future studies of this treatment approach. In addition, we used only a single injection of  $^{211}\text{At}$ -trastuzumab in our current mouse experiments, but because  $^{211}\text{At}$  has a short half-life, this agent could conceivably be administered via multiple injections to improve its efficacy. Further studies would be needed to evaluate the therapeutic efficacy and toxicity associated with a multiinjection approach.

## CONCLUSION

$\alpha$ -RIT using  $^{211}\text{At}$ -trastuzumab is efficacious in a clinically relevant mouse model of LMGC lesions that overexpress HER2. We propose that this strategy holds promise as a therapeutic option for LMGC in human patients.

## DISCLOSURE

This work was supported in part by the Japan Society for the Promotion of Science (JSPS) (KAKENHI 17K10462 to Sumitaka

Hasegawa, 17J02307 to Huizi Keiko Li, 17H05093 to Satoshi Kodaira, JP16H06276 [AdAMS] to Sumitaka Hasegawa), and a research grant from the Astellas Foundation for research on metabolic disorders (to Sumitaka Hasegawa). No other potential conflict of interest relevant to this article was reported.

## ACKNOWLEDGMENTS

We thank Atsushi Tsuji for advice about biodistribution-based dose estimation, Shino Homma-Takeda for the inductively coupled plasma mass spectrometry measurements, Hisashi Suzuki for radioisotope production, Takashi Murakami (Saitama Medical University) for the MKN45/Luc cells, Masumi Abe for encouragement with this present research, and the members of the Radiation and Cancer Biology Group for helpful discussions and technical assistance.

## KEY POINTS

**QUESTION:** What is the potential of  $^{211}\text{At}$ -trastuzumab for treating HER2-positive LMGC?

**PERTINENT FINDINGS:** A single intravenous injection of  $^{211}\text{At}$ -trastuzumab significantly inhibited growth of LMGC in mice.

**IMPLICATIONS FOR PATIENT CARE:**  $^{211}\text{At}$ -trastuzumab has potential as a future LMGC treatment in humans.

## REFERENCES

- Bray F, Ferlay J, Soerjomataram I, Siegel RL, Torre LA, Jemal A. Global cancer statistics 2018: GLOBOCAN estimates of incidence and mortality worldwide for 36 cancers in 185 countries. *CA Cancer J Clin*. 2018;68:394–424.
- Sun Z, Zheng H, Yu J, et al. Liver metastases in newly diagnosed gastric cancer: a population-based study from SEER. *J Cancer*. 2019;10:2991–3005.
- Bang YJ, Van Cutsem E, Feyereislova A, et al. Trastuzumab in combination with chemotherapy versus chemotherapy alone for treatment of HER2-positive advanced gastric or gastro-oesophageal junction cancer (ToGA): a phase 3, open-label, randomised controlled trial. *Lancet*. 2010;376:687–697.
- Dang HZ, Yu Y, Jiao SC. Prognosis of HER2 over-expressing gastric cancer patients with liver metastasis. *World J Gastroenterol*. 2012;18:2402–2407.
- Jiang H, Li Q, Yu S, et al. Impact of HER2 expression on outcome in gastric cancer patients with liver metastasis. *Clin Transl Oncol*. 2017;19:197–203.
- Carter P, Presta L, Gorman CM, et al. Humanization of an anti-p185HER2 antibody for human cancer therapy. *Proc Natl Acad Sci USA*. 1992;89:4285–4289.
- Guner A, Yildirim R. Surgical management of metastatic gastric cancer: moving beyond the guidelines. *Transl Gastroenterol Hepatol*. 2019;4:58.
- Carlin S. Penetrating the barriers to successful alpha-radioimmunotherapy. *J Nucl Med*. 2018;59:934–936.
- Zalutsky MR, Pruszynski M. Astatine-211: production and availability. *Curr Radiopharm*. 2011;4:177–185.
- Li HK, Sugyo A, Tsuji AB, et al. Alpha-particle therapy for synovial sarcoma in the mouse using an astatine-211-labeled antibody against frizzled homolog 10. *Cancer Sci*. 2018;109:2302–2309.
- Li HK, Hasegawa S, Nakajima NI, Morokoshi Y, Minegishi K, Nagatsu K. Targeted cancer cell ablation in mice by an alpha-particle-emitting astatine-211-labeled antibody against major histocompatibility complex class I chain-related protein A and B. *Biochem Biophys Res Commun*. 2018;506:1078–1084.
- Palm S, Back T, Claesson I, et al. Therapeutic efficacy of astatine-211-labeled trastuzumab on radioresistant SKOV-3 tumors in nude mice. *Int J Radiat Oncol Biol Phys*. 2007;69:572–579.
- Li HK, Morokoshi Y, Nagatsu K, Kamada T, Hasegawa S. Locoregional therapy with alpha-emitting trastuzumab against peritoneal metastasis of human epidermal growth factor receptor 2-positive gastric cancer in mice. *Cancer Sci*. 2017;108:1648–1656.
- Choi J, Vaidyanathan G, Koumariou E, Kang CM, Zalutsky MR. Astatine-211 labeled anti-HER2 5F7 single domain antibody fragment conjugates: radiolabeling and preliminary evaluation. *Nucl Med Biol*. 2018;56:10–20.
- Nagatsu K, Minegishi K, Fukada M, Suzuki H, Hasegawa S, Zhang MR. Production of  $^{211}\text{At}$  by a vertical beam irradiation method. *Appl Radiat Isot*. 2014;94:363–371.
- Homma-Takeda S, Nishimura Y, Terada Y, Ueno S, Watanabe Y, Yukawa M. Tin accumulation in spermatozoa of the rats exposed to tributyltin chloride by synchrotron radiation x-ray fluorescence (SR-XRF) analysis with microprobe. *Nucl Instrum Methods Phys Res B*. 2005;231:333–337.
- Sudo H, Tsuji AB, Sugyo A, et al. Preclinical evaluation of the acute radiotoxicity of the alpha-emitting molecular-targeted therapeutic agent  $^{211}\text{At}$ -MABG for the treatment of malignant pheochromocytoma in normal mice. *Transl Oncol*. 2019;12:879–888.
- Eckerman KF, Endo A. *MIRD: Radionuclide Data and Decay Schemes*. 2nd ed. Society of Nuclear Medicine and Molecular Imaging; 2008:616, 624.
- Sgouros G, Roeske JC, McDevitt MR, et al. MIRD pamphlet no. 22 (abridged): radiobiology and dosimetry of alpha-particle emitters for targeted radionuclide therapy. *J Nucl Med*. 2010;51:311–328.
- Kodaira S, Li HK, Konishi T, Kitamura H, Kurano M, Hasegawa S. Validating alpha-particle emission from  $^{211}\text{At}$ -labeled antibodies in single cells for cancer radioimmunotherapy using CR-39 plastic nuclear track detectors. *PLoS One*. 2017;12:e0178472.
- Kodaira S, Morokoshi Y, Li HK, Konishi T, Kurano M, Hasegawa S. Evidence of local concentration of alpha-particles from  $^{211}\text{At}$ -labeled antibodies in liver metastasis tissue. *J Nucl Med*. 2019;60:497–501.
- Yasuda N, Namiki K, Honma Y, et al. Development of a high speed imaging microscope and newsoftware for nuclear track detector analysis. *Radiat Meas*. 2005;40:311–315.
- Makino H, Kunisaki C, Izumisawa Y, et al. Indication for hepatic resection in the treatment of liver metastasis from gastric cancer. *Anticancer Res*. 2010;30:2367–2376.
- Kim HR, Cheon SH, Lee KH, et al. Efficacy and feasibility of radiofrequency ablation for liver metastases from gastric adenocarcinoma. *Int J Hyperthermia*. 2010;26:305–315.
- Luo Z, Rong Z, Huang C. Surgery strategies for gastric cancer with liver metastasis. *Front Oncol*. 2019;9:1353.
- Heyerdahl H, Abbas N, Sponheim K, Mollatt C, Bruland O, Dahle J. Targeted alpha therapy with  $^{227}\text{Th}$ -trastuzumab of intraperitoneal ovarian cancer in nude mice. *Curr Radiopharm*. 2013;6:106–116.
- Jiao R, Allen KJH, Malo ME, et al. Evaluation of novel highly specific antibodies to cancer testis antigen Centrin-1 for radioimmunotherapy and radioimmunotherapy of pancreatic cancer. *Cancer Med*. 2019;8:5289–5300.